3D Inverse modeling of EM-LIN data to investigate coastal sinkholes in Quintana Roo Mexico

Luis Eduardo Ochoa-Tinajero[1], Marco Antonio Perez-Flores[2], Almendra Villela y Mendoza[3]

[1]Posgrado en Ciencias de la Tierra, CICESE
[2]Dpeto. De Geofisica Aplicada, CICESE, Ensenada, México
[3]Universidad Autónoma de Baja California (UABC)

Correspondence to: Marco Pérez-Flores (mperez@cicese.mx)

Abstract. In southern Mexico at the Yucatan Peninsula (YP), cities and towns are settled on a platform of calcareous sedimentary sequence which has originated a wide formation of sinkholes, underground rivers and caverns due of karst process. The anthropogenic activities threat the only source of fresh water supply which is located in a regional unconfined aquifer; there are not lakes and rivers. For sustainable use of these resources at the YP, it is required to develop mathematical tools to help the groundwater modeling. In order to determine the geometry of the aquifer as the positions of caves, sinkholes and underground rivers we have developed software to invert three-dimensional electromagnetic low-induction numbers (3D EM-LIN) data for a set of profiles at arbitrary angle. In this work we have explored with the aid of EM-LIN geophysical method, the Chac-Mool sinkhole system at the state of Quintana Roo, Mexico. We have performed inverse modeling in 3D using the EM-34 instrument for vertical and horizontal magnetic dipoles. The 3D inversion process gives us models that allow us to correlate the path of the underground rivers with the subsurface electrical resistivity. In this work we have shown that inverse modeling of EM-LIN data is necessary to explore and understand coastal karst systems.

1 Introduction

The main source of fresh water in the YP is a regional unconfined karstic aquifer constituted by sedimentary limestones (Bauer-Gottwein et al., 2011). Karstic aquifers are extremely vulnerable to contaminants due their high permeability; the rapidly growth of the population in Quintana Roo and coastal touristic activities threat the only source of fresh water supply (e.g. Richards, D., & Richards, S. 2007).

In order to guarantee the sustainable use of these groundwater resources it is necessary to have knowledge of the hydrogeological characteristics such as geometry and positions of caverns and sinkholes as well as the depth of the fresh /salt water mixing zone (halocline).

Sinkholes are naturally geological features that connect the surface with the underground of karstic terrains and are formed when rain water dissolve limestone creating underground voids (Coskun, 2012).

Many of these features have been reported before by scuba divers and the Quintana Roo Speleological Survey has performed underground maps with scientific and touristic purposes in the Riviera Maya. However, geophysical techniques have been

barely applied as non-invasive methods for exploration over this area (e.g. Beauer-Gottwein et al. 2011; Gondwe et al. 2010; Estrada-Medina et al. 2010). It is well known that electrical resistive tomography has shown good results to explore karst e.g (Chalikakis et al 2011; Ahmed y Carpenter 2003), however in this region the lack of soil on this hard-limestone ground difficult the electrodes placing which results in a complicate and time consuming problem, making even more

5 expensive the data collection. New approaches in geophysical and coastal karst prospecting are therefore required in order to protect and develop future sustainability plans in the YP.

In this study we aim to investigate the application of a novel approach by using electromagnetic methods in the low-induction numbers limit (EM-LIN) and apply 3D geophysical inverse modeling (Perez-Flores et al., 2012) with the goal of set up a conceptual model of a sinkhole system and to get a wide knowledge of the site geomorphology. Moreover, the

10 methodology and results will also help as tool of management in the coastal zones of Quintana Roo due these are important for touristic activities which demands accurate knowledge for prospect plans of future development.

We did not find references for EM-LIN methods for karst systems, but we found DC and aero TDEM method applied in the Sian-Kan natural reserve (Supper et al. 2009). They also took EM-34 measurements, but they did not do any further processing or inverse modeling interpretation.

15 **1.1 Study area**

2 This research was done in the Yucatan Peninsula (YP), which is the emerged part of great Yucatan platform and 150,000 km^2 of 300,000 km^2 are largely karstified (Bauer-Gottwein et al., 2011). From the geological point of view, the YP is a platform constituted by a sequence of calcareous sediments (Bonet y Butterlin, 1962) and characterized by mountains and surface rivers absence. A review of the YP karst aquifer is well described by Bauer-Gottwein et al.

20 (2011) and an extend description of coastal cave development by Smart et al. (2006).

3 We took a study area that covers the Chac-Mool sinkhole and it is located 20 km southward Playa del Carmen in QR state at approximately 20° 30' 46.37" N and 87° 14' 49.32" W (Fig. 1). The area covers an extension of 1 km^2 and it is full covered by dense vegetation. The ground is heterogeneous and presents three types of porosity. The QR state receives around 1,200 mm of annual precipitation and topography varies between 5 m and 15 m over the sea level

25 (CNA, 2016). The hydraulic gradient in southern Playa del Carmen was estimated in 58-130 mm/km (Beddows, 2004). Chac-Mool sinkhole is located 9 m over sea level. This site is lack of soil and it is constituted by hard limestone rocks. Due to its proximity to the coast (2 km) is penetrated by the sea water. Such an intrusion oscillates depending on ties and rain recharge (Beddows, 2004). Chack-Mool is a sinkholes complex where it is assumed that two underground rivers connect the Little-Brother sinkhole and the Air-Dome sinkhole. The (x, y) river trajectories are known in some parts by

30 scuba diver maps (Quintana Roo Speleological Survey QRSS) but other parts remain unknown as well as the vertical components. It is possible that the entire rock matrix is saturated of fresh/brackish water through the porosity and small conduits. The electrical resistivity will not be very large.
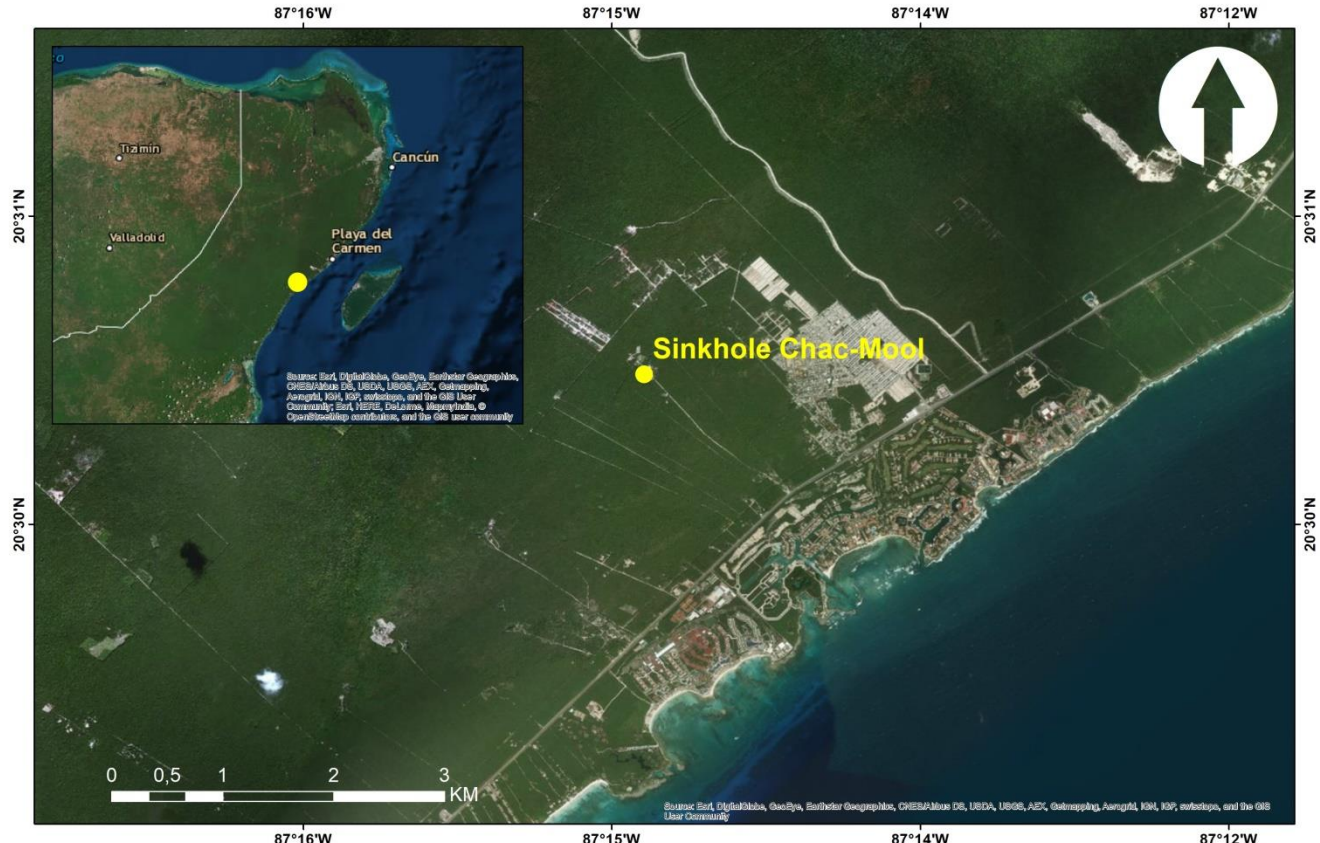
Figure 1. Study area: Chack-Mool sinkhole in the Quintana Roo state, Mexico.

1.2 Electromagnetic survey

In September 2015, we carried out a field trip over the study area. We took seven profiles with the EM34 (Geonics)
5   instrument that operate under the LIN domain as described in McNeill (1980). The main reason we are using EM-34 is
because it is easy and fast to take data in terrains with lack of soil without loss of accuracy, making faster the field-work in
tough terrains.

The principle consist in to pass an alternating current of constant frequency f through a coil (transmitter) which will generate
a primary electromagnetic field (H_p) that induces electrical currents in the conductive bodies embedded in the subsoil
10 (following Faraday's Law). Then a secondary electromagnetic field in the subsoil (H_s) is created due these conductive
bodies inside a half-space media. These two fields will differ in amplitude and phase and will be detected by a coil (receiver)
separated by a distance s(m) from the transmitter. The induction number N is defined as the quotient between s(m) and the
skin depth δ(m) as $N = s(m) / \delta(m)$. At low-induction numbers N<1 the imaginary part of H_s/H_p is a straight line whose

slope is the conductivity of a homogeneous half-space. Because of the real ground is not homogenous, we speak of an apparent conductivity $\sigma_a = (4/\omega\mu_0 S^2)(H_s/H_p)$.

It is usual to use both loops (source and receiver) in a coplanar way. We have two possible arrays, when both loops are parallel to the earth surface (vertical magnetic dipoles, HMD) and another when both loops are perpendicular to the earth

5 surface (horizontal magnetic dipole, HMD). For both arrays we can extend the separation between loops from 10 m, 20 m and 40 m. In this research the measurements were taking along 6 lines (Fig. 2) and every 5 m. Due the dense vegetation of the jungle it was not possible to locate profiles anywhere, instead we took the available paths around the sinkholes Chack-Mool and Little Brother. Then, we tried to follow straight lines thinking in doing 2D inversion for every data profile, but then we realized that six of the profiles distributions were more or less covering a rectangular area. Therefore, we performed

10 a 3D inversion in addition of the 2D model profiles (not presented here). For the 3D inverse modeling we followed Perez-Flores et al. (2012) method, but this algorithm was designed to parallel or perpendicular data profiles between them. They do not run for arbitrary angles like these profiles (Fig. 2). Later, we will show how we modified the equations for arbitrary angle data profiles. The six profiles (1 to 6) length varies between 50 m and 140 m (Fig. 2).

15

Figure 2. EM survey on the Chac-Mool sinkhole. Numbered profiles crossing the hidden rivers. With white wide line are the sinkholes exposed

1.3 Inverse modeling

We assume the EM data (apparent conductivity σ_a) as a weighted average of the subsurface electrical conductivity distribution, as described by Pérez-Flores et al. (2004).   We relate the apparent conductivity (σ_a) with the true subsurface conductivity (σ) thought a weighting function (that is the   Green function and electric field product) by using the approximate integral equation formulated by Pérez-Flores et al. (2001):

$$\sigma_a(\boldsymbol{r_2}, \boldsymbol{r_1}) \cong -\frac{16\pi s}{\omega\mu_0 m} \int_v \; \boldsymbol{G}(\boldsymbol{r_2}, \boldsymbol{r}, \sigma_0) \cdot \boldsymbol{E}(\boldsymbol{r}, \boldsymbol{r_1}, \sigma_0)\sigma(\boldsymbol{r})dv \tag{1}$$

Where $\boldsymbol{r_1}$ and $\boldsymbol{r_2}$ are the source and the receiver positions, $\boldsymbol{G}$ is the Green function for a homogeneous media due to a point electric source in $\boldsymbol{r}$ and measured in the magnetic receiver and $\boldsymbol{E}$ is the electric field for a homogeneous media due to the point magnetic source. Equation (1) is an approximation for low conductivity contrasts and it is very useful for inversion, where $\boldsymbol{G}, \boldsymbol{E}$ and σ_a are known, remaining $\sigma(\boldsymbol{r})$ as the unknown.

For inversion we have to considerer how the magnetic dipoles are used, we have the Vertical and horizontal magnetic dipoles (VMD and HMD respectively) arrays as describer in Pérez-Flores et al. (2012). The integral equation for the vertical magnetic dipoles (VMD) is,

$$\sigma_{a,z}(\boldsymbol{r_1}, \boldsymbol{r_2}) \cong -\frac{16\pi s}{\omega\mu_0 m_z} \int_v \; \boldsymbol{G}_{H_z}(\boldsymbol{r}, \boldsymbol{r_2}) \bullet \boldsymbol{E}_{H_z}(\boldsymbol{r}, \boldsymbol{r_1})\sigma(\boldsymbol{r})dv \tag{2}$$

For HMD the integral equation in y direction is given by:

$$\sigma_{a,y}(\boldsymbol{r_1}, \boldsymbol{r_2}) \cong -\frac{16\pi s}{\omega\mu_0 m_y} \int_v \; \boldsymbol{G}_{H_y}(\boldsymbol{r}, \boldsymbol{r_2}).\boldsymbol{E}_{H_y}(\boldsymbol{r}, \boldsymbol{r_1})\sigma(\boldsymbol{r})dv \tag{3}$$

And   HMD in x direction is given by:

$$\sigma_{a,x}(\boldsymbol{r_1}, \boldsymbol{r_2}) \cong -\frac{16\pi s}{\omega\mu_0 m_x} \int_v \; \boldsymbol{G}_{H_x}(\boldsymbol{r}, \boldsymbol{r_2}).\boldsymbol{E}_{H_x}(\boldsymbol{r}, \boldsymbol{r_1})\sigma(\boldsymbol{r})dv \tag{4}$$

The expression for $\boldsymbol{G}_{H_z}, \boldsymbol{E}_{H_z}, \boldsymbol{G}_{H_y}, \boldsymbol{E}_{H_y}, \boldsymbol{G}_{H_x}$ and $\boldsymbol{E}_{H_x}$ can be consulted in Perez-Flores et al. (2012). VMD profiles can run for any angle, but HMD runs only in y (90^0) or x (0^0) directions (Eq. 4 and 5). A problem is when we have arbitrary direction profiles as it happened around the Chac-Mool sinkhole (Fig. 3). So, we had to modify Eq. (4 and 5) in order to accept arbitrary angle profiles.

Using a simply notation for $\boldsymbol{E}$ and $\boldsymbol{G}$ in terms of their vector components, we have for y direction HMD,

$$\boldsymbol{G}_{H_y}(\boldsymbol{r}, \boldsymbol{r_2}) = d\hat{\imath} + e\hat{\jmath} \,, E_{H_y}(\boldsymbol{r}, \boldsymbol{r_1}) = \; a\hat{\imath} + b\hat{\jmath} \tag{5}$$

Similarly, along the x direction,

$$G_{H_x}(\boldsymbol{r}, \boldsymbol{r}_2) = e\hat{\imath} + f\hat{\jmath} \, , E_{H_x}(\boldsymbol{r}, \boldsymbol{r}_1) = \ b\hat{\imath} + c\hat{\jmath} \tag{6}$$

When we rotate Eq. (3) in 90^0, this becomes Eq. (4). So, we can find $\boldsymbol{E}$ and $\boldsymbol{G}$ in terms of their rotated components.

$$\begin{pmatrix} E_x \\ E_y \end{pmatrix} = \begin{pmatrix} cos\theta & sen\theta & 0 \\ & cos\theta & sen\theta \end{pmatrix} \begin{pmatrix} a \\ b \\ c \end{pmatrix},$$

$$\begin{pmatrix} G_x \\ G_y \end{pmatrix} = \begin{pmatrix} cos\theta & sen\theta & 0 \\ & cos\theta & sen\theta \end{pmatrix} \begin{pmatrix} d \\ e \\ f \end{pmatrix} \tag{7}$$

If a HMD profile runs at 0^0, $(E_x, \ E_y)$ becomes $\boldsymbol{E}_{H_y}$ from Eq. (3). If the profile runs at 90^0, $(E_x, \ E_y)$ becomes $\boldsymbol{E}_{H_x}$ from Eq. (4).

Thus, for an arbitrary angle profile, Eq. (3 and 4) become a single one,

$$\sigma_a(\boldsymbol{r}_1, \boldsymbol{r}_2) = -\frac{16\pi s}{\omega\mu_0 m_B} \int [G_x(\boldsymbol{r}, \boldsymbol{r}_2)E_x(\boldsymbol{r}, \boldsymbol{r}_1) + G_y(\boldsymbol{r}, \boldsymbol{r}_2)E_y(\boldsymbol{r}, \boldsymbol{r}_1)]\sigma(\boldsymbol{r})dv \tag{8}$$

Terms *(a, b, c, d, e, f)* can be obtained from Perez-Flores et al. (2012).

For the 3D inversion, we used Eq. (8) for the HMD profiles and Eq. (2) for the VMD profiles. We used 10, 20 and 40 m for the source-receiver separations for VMD and the same separations for HMD in every profile. We inverted together the whole sets of data in order to get a single 3D conductivity model. We simulated the heterogeneous half-space as a conglomerate of rectangular prisms. We assumed that conductivity is constant in every single prism but unknown. Eq. (2) and (8) can be written as a linear equations system, and in a matrix way,

$$\boldsymbol{\sigma}_a = \boldsymbol{W}\boldsymbol{\sigma} \tag{9}$$

Where $\boldsymbol{\sigma}_a$ represents the column vector of apparent conductivities, matrix $\boldsymbol{W}$ contains the weights or products of the Green function and electric field and it is partitioned for VMD and HMD and $\boldsymbol{\sigma}$ represents the column vector of the real conductivities (unknowns). We use quadratic programing to minimize the next objective function $\boldsymbol{U}$

$$\boldsymbol{U}(\boldsymbol{\sigma}) = \frac{1}{2}\left\|\boldsymbol{\sigma}_a - \mathbf{W}\boldsymbol{\sigma}\right\|^2 + \frac{1}{2}\beta\left\|\mathbf{D}\boldsymbol{\sigma}\right\|^2$$

$$\boldsymbol{\sigma}_{lower} < \boldsymbol{\sigma} < \boldsymbol{\sigma}_{upper} \tag{10}$$

Matrix $\boldsymbol{D}$ represents the first order spatial derivatives of the contiguous prism conductivities. Parameter β controls the smooth of the 3D conductivity model; when it is low, we got a roughness 3D model.
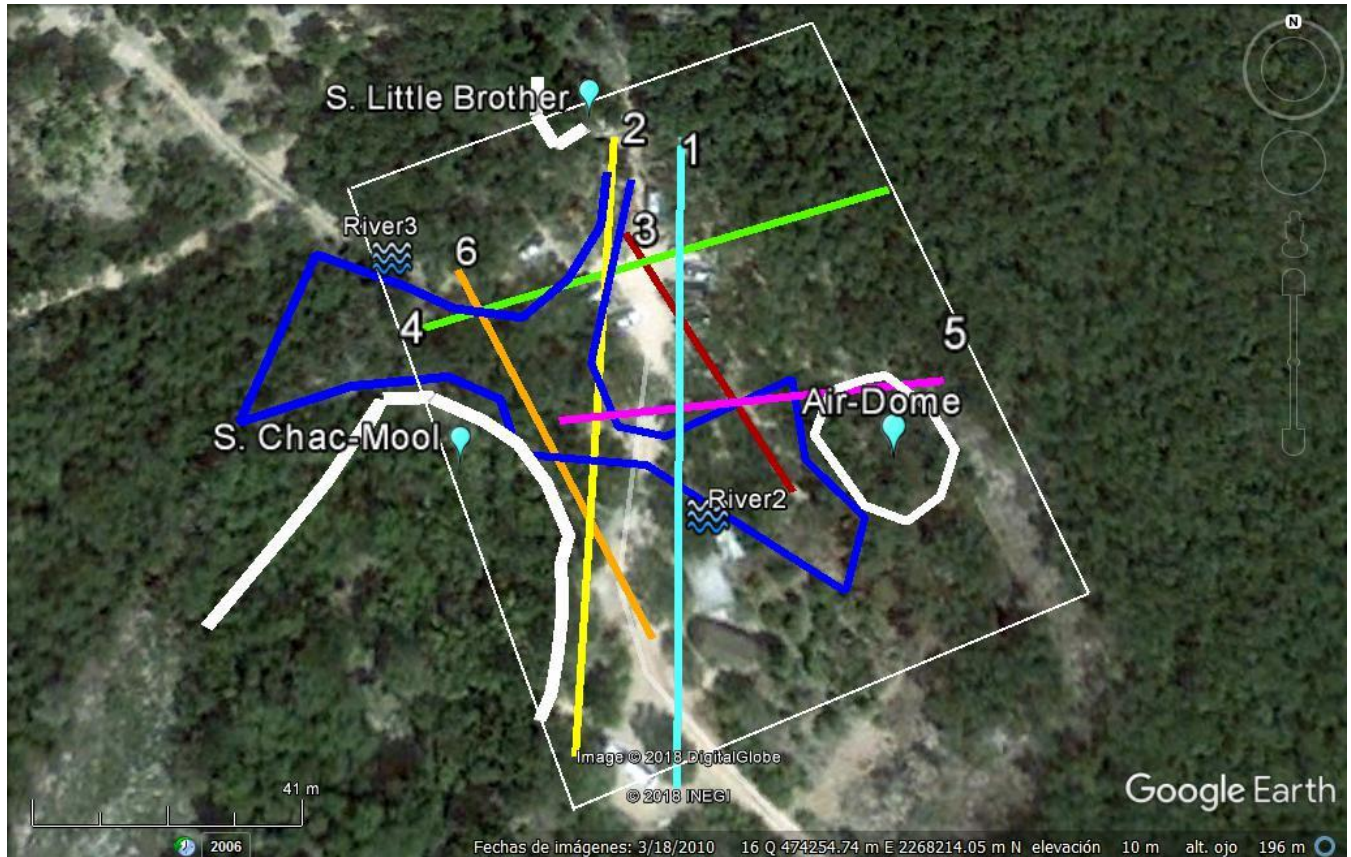
Figure 3. Profiles crossing the hidden rivers on the sinkhole area (numbered). The white rectangle is the 3D modeling area. White wide lines are the sinkholes exposed. Dark blue lines are the suggested rivers paths.

2 Resistivity cross-sections over the 3D model.

For the 3D inverse modeling we used a (x, y, z) grid of prisms, assuming constant conductivity in every one. We performed the inverse modeling choosing $\Delta x = \Delta y = 2.5$ m in the (x, y)-directions due the EM measurement was taken every 5 m; a variable discretization of Δz was chosen as (0, 2, 5, 8, 12, 18, 25, 35 and 50 m) and β=0.01 as the smoothness factor.

Conductivity is the unknown, but we prefer to show results in resistivity. In Fig. 4 we present the 3D resistivity model after the inversion process of the whole sets of data. In this figure we present the interpolated resistivity cross-sections under the six profiles. Blue are resistive areas and red low resistive. There are spaces between profiles that have no data. In those areas the 3D model is not very confident. Therefore, we better show the model where the data are as a first approach. There is a very good coherence where the model crosses. In this figure are shown the irregular paths of the two rivers. They follow very intricate paths. We think that there are narrower river branches that have not yet discovered by the divers. It is

interesting that some paths were market bellow the resistive areas. Meaning that maybe the subterranean rivers are far enough from surface, making the roof more stable structurally or maybe there are air-filled caves over the water table. We must remember that a typical cave in this area (near the coast) consists of an empty space close to the limestone roof (very resistive), then fresh water (lower resistivity), the halocline (fresh and salty water mix), and at the bottom, salty water (the

5   lowest resistivity surrounded by saturated limestones.

In Fig. 5 we show the six cross-sections done to the 3D resistivity model. Cross-section (a) correspond to the profile 1 model, cross-section (b) to profile 2 and so on. In every profiles are signed with a white dot the interpolated (x, y, z) hidden-rivers reported by the scuba divers. They do not specify where this coordinate was taken inside the cave. It is a broad record of the diver's path. Therefore, we show on the resistivity image the interpolated location, that it is even more inaccuracy.
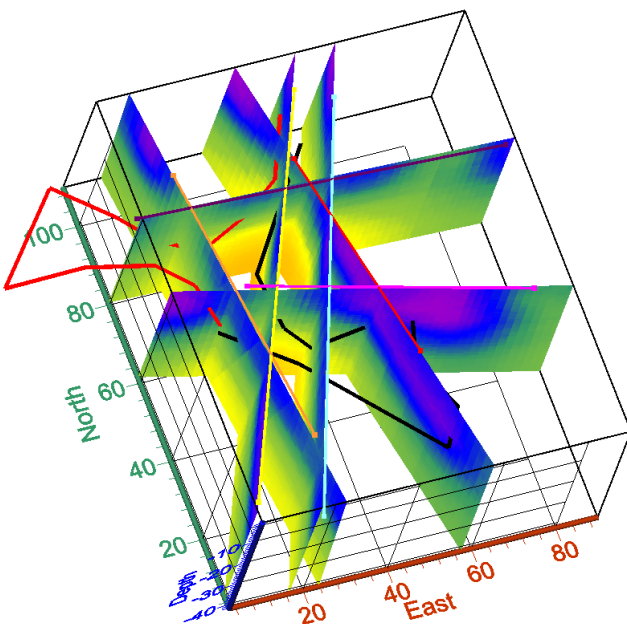
Figure 4. 3D resistivity model for Chac-Mool sinkhole. Here we just present the cross-sections distribution where the profiles run. The red and black irregular lines represent the hidden rivers.

15   Looking the six-resistivity cross-sections, we can see that most of the rivers crosses show a green color over them. Meaning perhaps that the subterranean rivers is close to the surface and therefore the roof thickness is thinner, making those areas more sensible for roof sinking. Profile 1 cross-section (Fig. 5a) shows three crosses: at x=18m shows a thinner roof, the others a thicker roof. Profile 2 (Fig. 5b) shows a green color, meaning thinner roofs. Profile 3 (Fig. 5c) show one river crossing shallow and another deeper. We can see that a shallower subterranean river is well detected (green color) by the

20   EM-LIN equipment but it is not obvious when this is deeper. In profile 4 (Fig. 5d) they show three crossings with green color. But the diver's depth reported is not very shallow; however this could be explained by considering that water table is

8m depth and the electromagnetic response in that point is higher due the rivers contribution. Profile 5 (Fig. 5e) shows three crossings, two deeper (between z=20 and z=30) and one shallower (z=15m). The deeper are consistent with the diver's depth reported and the thicker roof obtained by the resistivity model, however at x=25m the river seems to be 10m deeper, this could be explained, considering that there is a huge hard rock (very resistive) that could be affecting the response and, in the

5 model, seems to be 10 m deeper. The last profile 6 (Fig. 5f) shows a shallower river and a deeper one, resistivities are consistent with the position of this one.

We know that divers pass throughout a tunnel. In Fig. 5 we propose a broad suggestion about those tunnels (rectangular polygon). Giving an explanation to the colors in Fig. 5, we can think that blue can correspond to dry limestone roofs or dry

10 limestone plus air-filled caves at the top of the tunnels. Green color is so smooth that surely contains clean water, but we do not know the shape. Also, the resistivity cross-section shows green when the subterranean rivers are shallow. We do not have a narrow blue color plus a green color. That is maybe, because the lowest separation source-receiver at the EM34 is 10 m. In some way the true conductivity estimated continues being an average. Maybe if we could use a lower separation, we could resolve a thinner blue color roof and then a green color from the clean water. The transition from green to red (yellow) could

15 be the transition from clean water to salty water. We expect that clean water is stratified inside the tunnels with the salty water at the bottom.

We drew the tunnels with the idea to emphasize that EM34 have not the resolution to sharply isolate tunnels from the bedrock. An explanation is that unaltered bedrock (limestone) is saturated of clean water at the shallow depths and saturated

20 of salty water at the deeper parts. So, there are not a large horizontal resistivity changes between the tunnels and the bedrock. With the aerial EM we will have even a lower resolution, but we could see in a faster way where the subterranean rivers are when they are close to the surface in a horizontal map. However, a non-quantitative roof thickness images and not a better resolution in depth would be expected.

In profile 4 (Fig. 5d) there is a green color sector close to x=70 m. It is possible that a shallow subterranean river pass very

25 close to surface and it was not yet mapped by divers.
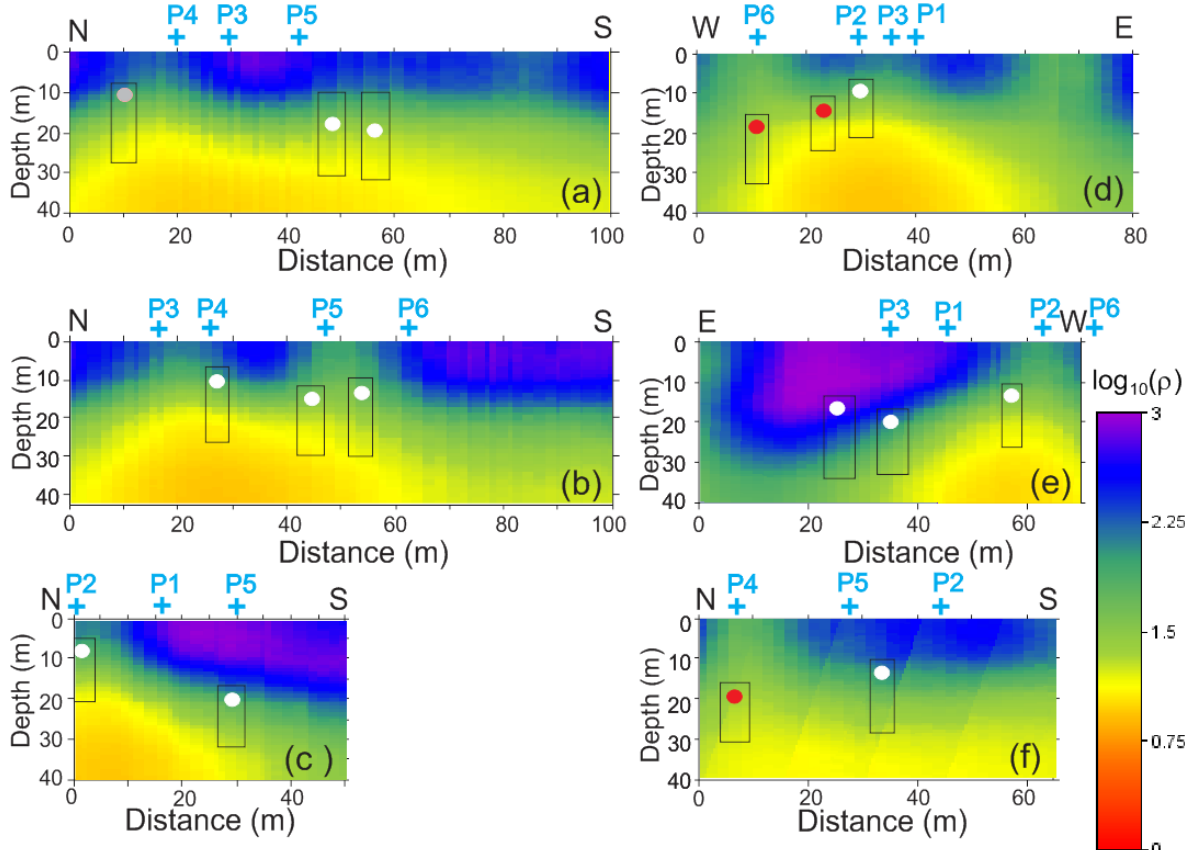
Figure 5. Cross-sections of the 3D resistivity model under profiles 1 to 6. Units are base 10 logarithm of the resistivity. Blue colors are more resistive areas and red colors the least resistive. Blue numbers signs the other profiles crossings. Red dots signs where the scuba divers suggest the red color river cross (figure 4). White dots for the black color river cross (figure 4). Square polygon is a broad suggestion of the river tunnels.

2.1 Isometric of the 3D resistivity model.

Chac-Mool sinkhole is a complex of three small sinkholes (Air-Dome, Little Brother and Chac-Mool itself). According to divers, there are two underground rivers whose position in (x,yz) varies. Their vertical variation may cause the thinner of the limestone roof and therefore sinking. According to the cross-section in Fig. 6, the EM-LIN equipment can not sharply desitinguish between the river tunnels and the bedrock, maybe because there is not enough resitivity change, meaning that bedrock limestones are saturated of water and therefore under the chemical disolution process. Looking the isometric of the 3D resistivity model (Fig. 6) we can see the spatial distribution of the three sinkholes inside the complex. With two kind of blue the two proposed rivers and treir paths. We also see the location of the five profiles of EM-LIN data.

The blue and green surfaces are equal-resistivity surfaces of the 3D model (160 ohm-m). The blue one pretends to show the bottom topography of the limestone roof. This resistive layer may contain unaltered limestone plus air-filled caves. It is very interesting that this layer outcrops where underground rivers are very shallow, and those paths are very coincident where the rivers are shallow. This surface does not outcrop where the sinkholes are, because there are not data there. They were gaps

5   where it was impossible to take data. We did not want to manipulate the 3D model to obligate the model to outcrops where sinkholes are, but we can by mean of quadratic programing in the minimization process of equation (10). But we rather want to see a non-manipulated result.

It is also interesting that in the middle of the study, there is a resistive massif (MR letters), where the roof appears to be very thick. That means that that zone is the least hazard area for roof collapse.

10   The green surface pretends to be the surface where the clean water is located (80 ohm-m). But this surface also outcrops where blue surface outcrops. Maybe because the EM-LIN source-receiver separation was too large (10 m) and we are looking a kind of resistivity average between the roof (resistive) and the clean water (less resistive). But this happens just where the roof is very thin. We must be careful with this model where no data exist.
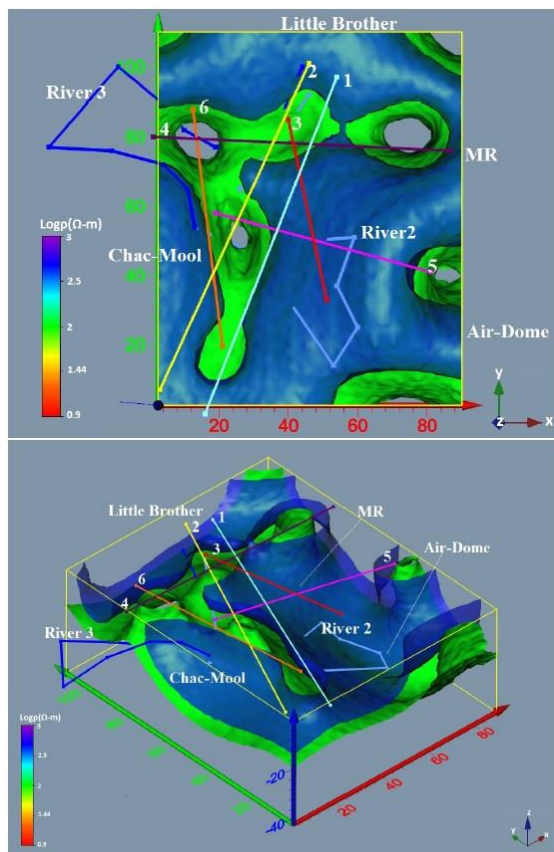
15   Figure 6. Isometric of the 3D resistivity model. Iso-resistivity surfaces. Blue represent the bottom topography of the underground roof. Green the surface of the clean water.

3. Conclusions

In this research we are exploring the Chac-Mool sinkhole complex by mean of electromagnetic methods operating at low-induction numbers (EM-LIN). These methods consist of a source loop and a received loop working coplanar to the Earth
5   surface (VMD) and perpendicular (HMD). These two polarizations look the Earth in a different way. That is why; we used both arrays in order to do joint inversion and to obtain a single three-dimensional (3D) resistivity model. Those equations were already published for a mesh of perpendicular and parallel profiles, but not for arbitrary angle profiles. In this research the profiles were taken inside the jungle and we took the advantage of already made walk paths, but these were in arbitrary angles. We had to modify the existing equations, arriving to a more general set of equations.

10   We did 3D inversion of both VDM and HDM arrays arriving to a single 3D resistivity model. The cross-sections of this 3D model show where the underground rivers cross. Where the underground rivers approach the surface may create a hazard of roof collapse. We also see the distribution of the clean and salty water distribution and their contact or the transition surface (halocline). We see that rivers must run along tunnels but resistivity of those tunnels do not sharply differ from resistivity of the bedrock, meaning that they are also saturated of water (clean and salty depending the depth). The isometric shows that
15   resistive iso-surface corresponds with the bottom topography of the underground roof. At the center of the area this roof seems very thick making this area very stable for sinking hazard. This isometric also shows that where the blue iso-resistivity surface outcrops is where underground rivers close to surface.

This EM-LIN technique is very efficient, fast and cheap for exploring over hard rock sinkhole areas. We can get the geometry of the underground rivers and the distribution between clean and salty water.

20

References

Ahmed, S. and Carpenter, P. J.: Geophysical response of filled sinkholes, soil pipes and associated bedrock fractures in thinly mantled karst, east-central Illinois, Environmental Geology, 44, 705-716, 2003.

25   Bauer-Gottwein, P. Gondwe, B.R. Charvet G., Marin, L.E. Robellodo-Vieyra, M. and Meresiz-Alonso, G.: Review: The Yucatan Peninsula karst aquifer, Mexico, Hidrogeology Journal, 19, 507-524, 2011.

Beddows, P. A.: Groundwater hydrology of a coastal conduit carbonate aquifer: Caribbean coast of the Yucatán Peninsula, México, PhD thesis, University of Bristol, 2004.

Bonet, F. Butterlin, J.: Stratigraphy of the northern part of the Yucatan Peninsula, Field trip to Peninsula of Yucatan guide
30   book, New Orleans Geological Society, New Orleans, LA, 1962.

Chalikakis, K. Plagnes, V. Guerin, R. Valois, R. and Bosch, F. P.: Contribution of geophysical methods to karst-system exploration: an overview, Hydrogeology Journal, 19, 1169-1180, 2011.

Comisión Nacional del Agua (CNA).: Resumen Técnico de las Condiciones Geohidrológicas del Estado de Quintana Roo, Comisión Nacional del Agua, Subgerencia Técnica, Gerencia Regional del Sureste, Mérida, Yucatán, México 2016.

COŞKUN, N.: The effectiveness of electrical resistivity imaging in sinkhole investigations. International Journal of Physical Sciences, *7*(15), 2012.

Estrada-Medina, H. Tuttle, W. Graham, R.C. Allen, M.F. and Jiménez-Osornio, J.J.: Identification of underground karst features using ground-penetrating radar in Northern Yucatán, México, Vadose Zone Journal, 9, 653-661, 2010.

5 Gómez-Treviño, E.: Nonlinear integral equations for electromagnetic inverse problems, Geophysics, 52, 1297–1302, 1987.

Gondwe, B.R. Lerer, S. Stisen, S. Marín, L. Rebolledo-Vieyra, M. Merediz-Alonso, G. and Bauer-Gottwein, P.: Hydrogeology of the south-eastern Yucatan Peninsula: new insights from water level measurements, geochemistry, geophysics and remote sensing, Journal of Hydrology, 389, 1-17. 2010.

McNeill, J.D.: Electromagnetic terrain conductivity measurement at low induction numbers, Technical Note TN-6, Geonics

10 Limited, 1980.

Pérez-Flores, M.A. Antonio-Carpio, R.G. Gómez-Treviño, E. Ferguson, I. and Méndez-Delgado, S.: Imaging of 3D electromagnetic data at low-induction numbers, Geophysics, 77, WB47-WB57, 2012.

Pérez-Flores, M.A. Méndez-Delgado, S. and Gómez-Treviño, E.: Imaging low-frequency and dc electromagnetic fields using a simple linear approximation, Geophysics, 66, 1067-1081, 2001.

15 Richards, D. and Richards, S.: Overview of the geology and hydrology of coastal Quintana Roo, AMCS Activ Newsl 30, 104–109, 2007.

Smart, P. L. Beddows, P. A. Coke, J. Doerr, S. Smith, S. and Whitaker, F. F.: Cave development on the Caribbean coast of the Yucatan Peninsula, Quintana Roo, Mexico, Geological Society of America Special Papers, 404, 105-128, 2006.

Supper, R., Motschka, K., Ahl, A., Bauer-Gottwein, P., Gondwe, B., Alonso, G. M., & Kinzelbach, W.: Spatial mapping of

20 submerged cave systems by means of airborne electromagnetics: an emerging technology to support protection of endangered karst aquifers, Near Surface Geophysics, *7*, 613-627, 2009.

25